Please cite as
Journal of Electronic Materials, 2014, DOI: 10.1002/pssa.201300130

Paradoxical enhancement of the power factor in polycrystalline silicon due to the formation of nanovoids

B. Lorenzi · D. Narducci* · R. Tonini · S. Frabboni · G.C. Gazzadi · G. Ottaviani · N. Neophytou · X. Zianni

Received: date / Accepted: date

B. Lorenzi
Dept. Materials Science, Univ. of Milano Bicocca, Milano, Italy
Tel.: +39 02 6448-5143
Fax: +39 02 6448-5400
E-mail: b.lorenzi2@campus.unimib.it

D. Narducci *(corresponding author)*
Dept. Materials Science, Univ. of Milano Bicocca, Milano, Italy
Tel.: +39 02 6448-5137
Fax: +39 02 6448-5400
E-mail: dario.narducci@unimib.it

R. Tonini
Dept. of FIM, Univ. of Modena and Reggio Emilia, Modena, Italy
Tel.: +39 059 2055249
Fax: +39 059 2055235
E-mail: rita.tonini@unimore.it

S. Frabboni
Dept. of FIM, Univ. of Modena and Reggio Emilia, Modena, Italy and CNR, Institute of Nanoscience – S3, Modena, Italy
Tel.: +39 059 2055259
Fax: +39 059 2055235
E-mail: stefano.frabboni@unimore.it

G.C. Gazzadi
CNR, Institute of Nanoscience – S3, Modena, Italy
Tel.: +39 059 2055323
Fax: +39 059 2055235
E-mail: giancarlo.gazzadi@unimore.it

G. Ottaviani
Dept. of FIM, Univ. of Modena and Reggio Emilia, Modena, Italy
Tel.: +39 059 2055263
Fax: +39 059 2055235
E-mail: giampiero.ottaviani@unimore.it

N. Neophytou
Institute for Microelectronics, Technical University of Vienna, Wien, Austria, and School of Engineering, University of Warwick, Coventry, UK
Tel.: +43 58801 36030
Fax: +43 58801 36099
E-mail: neophytou@iue.tuwien.ac.at

X. Zianni
Dept. of Aircraft Technology, Educational Institution of Sterea Ellada, Psachna, Greece and Dept. of Microelectronics, IAMPPNM, NCSR Demokritos, Athens, Greece
Tel.: +30 22280 99541
Fax: +30 22280 23766
E-mail: xzianni@gmail.com

Abstract Holey silicon has been considered a viable candidate as a thermoelectric material in view of its low thermal conductivity. However, since voids are efficient scattering centers not just for phonons but also for charge carriers, achievable power factors (PFs) are normally too low for its most common embodiment, namely porous silicon, to be of practical interest. In this communication we show that high power factors can indeed be achieved in nanoporous structures in highly doped silicon. High power factors, up to a huge 22 mW $K^{-2}m^{-1}$ (more than six times higher than bulk values), were observed in heavily boron doped nanocrystalline silicon films where nanovoids (NVs) were generated by He^+ ion implantation. Differently than in single-crystalline silicon where He^+ implantation leads to large voids, in polycrystalline films implantation followed by annealing at 1000 °C results in the formation of a homogeneous distribution of NVs with final diameters of about 2 nm and densities on the order of 10^{19} cm^{-3} with an average spacing of 10 nm. Its morphology shows silicon nanograins of 50 nm in diameter decorated by SiB_x 5-nm precipitates. We recently reported that PFs up to 15 mW $K^{-2}m^{-1}$ can be achieved in silicon-boron nanocomposites (without NVs) due to a simultaneous increase of the electrical conductivity and Seebeck coefficient. In that case, high Seebeck coefficient was achieved by potential barriers on the grain boundaries, and high electrical conductiv-

ity by extremely high doping values. The additional increase in the PF observed in the presence of NVs (that also include SiB_x precipitates) might be attributed to several possible reasons, currently under investigation. Experimental evidence is put forward to elucidate this paradoxical effect of NVs on silicon PF.

Keywords Silicon · Thermoelectricity · Nanovoids · Energy filtering

1 Introduction

In spite of its low thermoelectric (TE) efficiency, it would be highly desirable that silicon might qualify as a material for TE conversion due to the large scientific and technological know-how available on silicon, and because of the easy integrability of Si–based TE devices. As well known, the low TE efficiency of silicon is due to its high thermal conductivity (ranging from ≈ 130 W K^{-1}m^{-1} in intrinsic single-crystal silicon [1] to ≈ 25 W K^{-1}m^{-1} in nanocrystalline silicon [2]) and to its relatively low power factor (PF) (≤ 3 mW K^{-2}m^{-1} – although larger values, up to 6.3 mW K^{-2}m^{-1} at 350 K, were recently reported [3]). In previous papers [4–6] we have shown that, upon boron precipitation, highly boron-doped nanocrystalline silicon may reach PFs as high as 15 mW K^{-2}m^{-1} at 300 K. In order to decrease its thermal conductivity, the introduction of voids by He^+–implantation appears to be a viable route to explore, possibly with a marginal reduction of the hole conductivity. Previous literature [7,8] reported contrasting results, clearly suggesting the role of pore size and structure on both the PF and the thermal conductivity.

The aim of this paper is to report preliminary results obtained in the thermoelectric characterization of heavily doped nanocrystalline silicon implanted with He^+. It is shown that He^+ implantation followed by annealing leads to the formation of nanovoids that, rather unexpectedly, improve the material power factor. Although the data currently available are admittedly incomplete, the picture they fit in is consistent with models and results previously reported in heavily doped nanocrystalline silicon and may be supposed to raise interest in the thermoelectric community in view of the exceptionally high power factors.

2 Experimental

Silicon polycrystalline 450-nm thick films were deposited by chemical vapor deposition (CVD) onto oxidized single-crystal silicon substrates. Films were doped with boron by ion implantation (60 keV, 2×10^{16} cm^{-2}) to a nominal total boron concentration of 4.4×10^{20} cm^{-3} and submitted to a standard damage recovery treatment (1050 °C, 30 s in N_2). An aluminum 250-nm thick sacrificial layer was then deposited by sputtering onto the films that were further implanted with helium in a two-step process (90 keV, 4×10^{16} cm^{-2} + 58 keV, 1.5×10^{16} cm^{-2}). To prevent contamination and to match the 90 keV He end-of-range distribution within the poly layer, an aluminum layer was then removed by etching in HCl. Finally, a standard cleaning treatment (piranha etch, 90 °C, 30 min, followed by 3% mol. HF) was carried out prior to evaporating Al-Si 1% electrical contacts through a shadow mask. Thermal desorption spectra obtained at constant heating rate showed a behaviour similar to the single crystal case [9] with He fully desorbing at 800 °C.

Samples were submitted to annealing in argon to analyze the structural and functional evolution of the films. Metal contacts were removed by HCl etch prior to each annealing and redeposited afterward.

Samples for the Seebeck coefficient and the electrical conductivity measurements were 50×5 mm^2 rectangular chips while Hall measurements were carried out on 17×17 mm^2 samples with aluminum contacts evaporated on small areas in the four corners according to the Van der Pauw geometry. Hall measurements were carried out at room temperature (298 K) using a maximum magnetic field of 0.5 T. Accuracy was found to be better than ±1%. Precision was estimated, based on the deviation of contact design with respect to the ideal Van der Pauw configuration [10], to be $+0/-17\%$ for the Hall mobility and of $+18/-0\%$ for the carrier density p. Seebeck coefficient and electrical conductivity were measured using a home–built system. For the Seebeck coefficient measurements the integral method [11] was used, fixing the temperature of the cold contact at 20 °C while heating the other contact between 40 and 120 °C. Conductivity was determined by current-voltage characteristics at 20 °C. Each set of Seebeck coefficient measurements was repeated on the same sample at least three times to ensure data reliability. Also, charge transport coefficients were measured on nominally identical samples and found to be reproducible within ±10%. The whole experimental setup was calibrated toward single-crystal silicon samples of known doping level.

Cross-sections for electron microscopy (EM) analyses were prepared by both conventional and focused-ion beam lift-out methods. EM analyses were performed both in low-energy (30 keV) dark field scanning transmission EM (DF-STEM) and in high-energy (200 keV) transmission (TEM) mode. Low-energy analyses have

been performed with a FEI Strata235M (FEI Company, Hillsboro, OR, USA) equipped with bright field (BF)–dark field (DF) solid state detector. TEM and energy filtered electron spectroscopic images (ESI) have been performed with a JEM2011 electron microscope (Jeol Ltd., Tokyo, Japan) (spherical aberration coefficient 0.5 mm, chromatic aberration coefficient 1.1 mm) equipped with conventional LaB_6 electron source and an electron energy loss imaging filter GIF 200® (Gatan Inc., Pleasanton, CA, USA). This attachment allows to record both electron energy loss spectroscopy (EELS) data and ESI.

In order to evaluate the density of helium atoms effectively presents inside the silicon lattice Temperature Programmed Desorption (TPD) measurements were carried out after helium implant. TPD experiments, consisting in the measurement of the helium effusion rate during a thermal treatment in a temperature ramp with assigned heating rate, is an ideal technique to study the evolution towards stable cavities of vacancy–like defects in helium implanted silicon. It can actually give information about the kinds and the states of the structures where helium is trapped. TPD spectra were performed at a pressure of $\approx 10^{-6}$ mbar, with a ramp rate of 0.75 °C/s in the temperature range 80–800 °C.

3 Results

Heat treatments promote three simultaneous diffusion processes, namely *(a)* vacancy diffusion, leading to the final formation of nanovoids; *(b)* boron diffusion, resulting in its segregation at grain boundaries (GBs) and then eventually to its precipitation as a second phase; and *(c)* helium outdiffusion from silicon. As the three processes are characterized by different rates, several sets of sequential annealing cycles were carried out. In the first, we analyzed the variations of σ and α upon annealing of two hours in steps of 100 °C from 500 °C to 1000 °C. In the second one, a shorter cycle was implemented, sequentially annealing the samples for 2 h at 500 °C and 1000 °C only. We will refer to these two experiments as Exp1 and Exp2.

The evolution of the Seebeck coefficient α in Exp1 showed a trend closely reminiscent of that observed in non-He-implanted (nHeI) samples [4,6] (Fig. 1). Seebeck coefficient shows actually a rather abrupt increase upon annealing at 800 °C, reaching a topmost value of 0.45 mV/K after being annealed at 1000 °C. The electrical conductivity σ displays instead an almost linear increase with the annealing temperature T_a, quite different from that observed in nHeI specimens.

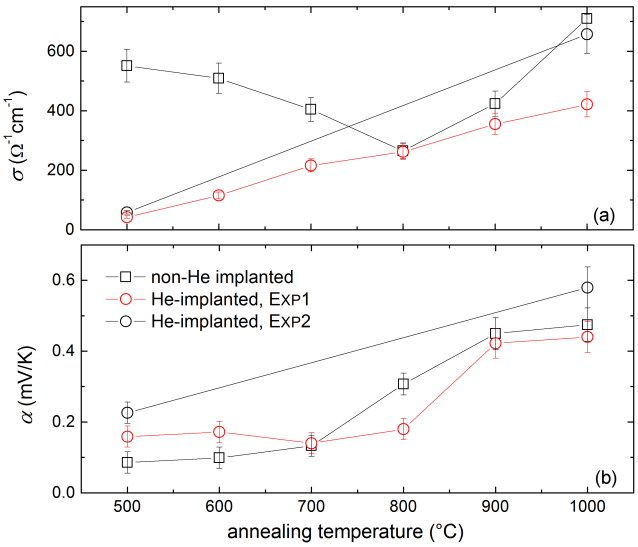

Fig. 1 *(a)* Electrical conductivity and *(b)* Seebeck coefficient vs. annealing temperature upon sequential annealing in Ar from 500 to 1000 °C in two-hour long, 100 °C steps (Exp1); and upon two-hour annealing at 500 and 1000 °C only (Exp2) compared to non-He implanted samples annealed in Ar from 500 to 1000 °C in two-hour long, 100 °C steps.

It is interesting to compare such a trend with that observed in Exp2. While both σ and α after annealing at 500 °C are similar in the two experiments, Exp2 leads to an electrical conductivity at 1000 °C closely comparable to that of the nHeI samples; while Exp1 results in a final σ value about half of that observed in the absence of helium implantation. On the contrary, the final Seebeck coefficient for Exp1 is equal to that of the nHeI material while Exp2 returns a final α value about 15 % larger.

To elucidate such differences, Hall effect measurements were carried out. We set to carry out the sequential annealing under conditions intermediate between Exp1 and Exp2 — namely 30–minute annealing from 500 to 1000 °C in 100 °C steps (Fig. 2). We will refer to this annealing cycle as to Exp3. As expected, the steady increase of σ observed in all He–implanted samples is apparently caused by the regular increase of the hole mobility μ, changing by almost a factor of four from the as–implanted to the fully cured film.

As of the carrier density, in nHeI specimens p reflected the diffusion–limited precipitation of boron from the supersaturated Si–B solid solution [4,5]. A different $p(T_a)$ trend is observed in Exp3, where actually p smoothly increase by a factor of five upon annealing up to 700 °C, still leveling to 10^{20} cm^{-3} – a value close to that measured in nHeI films – for higher annealing temperatures.

TPD analyses performed on as–implanted samples showed a total effusive helium fluence of 4.5×10^{16}

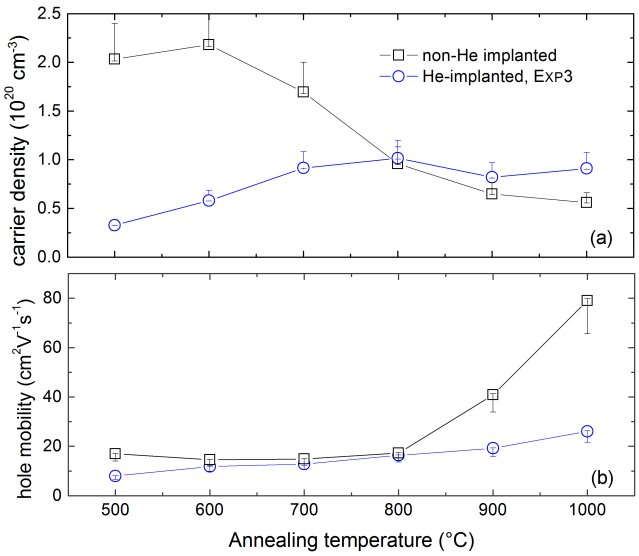

Fig. 2 *(a)* Carrier density and *(b)* hole mobility and vs. annealing temperature upon sequential annealing in Ar from 500 to 1000 °C in 30-minute long, 100 °C steps (Exp3).

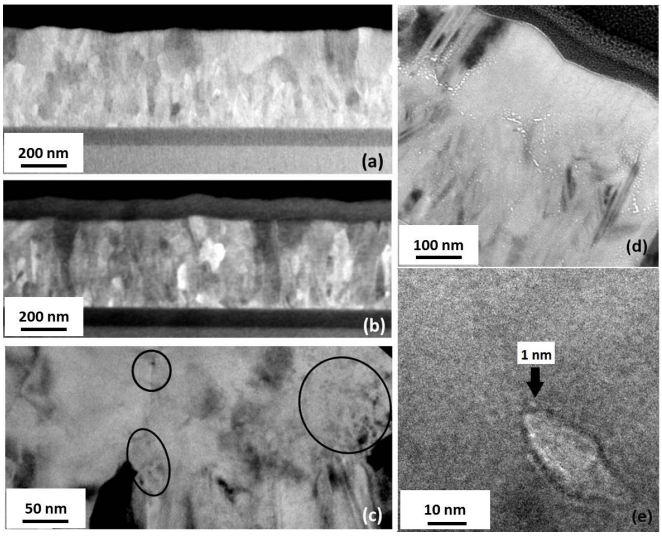

Fig. 3 (*a*) DF-STEM image of the as–deposited non-He implanted sample; (*b*) DF-STEM and (*c*) TEM bright field image of the same sample after annealing at 1000 °C. Circled areas in the TEM image mark diffraction contrast details relating to SiB_x precipitates. Note also the preservation of grain sizes upon annealing at high temperature. TEM images of He implanted sample upon annealing at 500 °C, two hours (*d*) and upon subsequent annealing at 1000 °C, two hours (*e*). Note the distribution of nanovoids throughout the grains, their size shrinking down to a sub-nanometric size when increasing the annealing temperature.

cm^{-2}. These results are compatible with those reported in literature on single–crystalline samples [12], showing no difference in the amount of helium implanted and outdiffused also in the polycrystalline case. A single outdiffusion peek was found at 780 °C.

TEM provided highlights on the formation of voids and precipitates. Helium implantation in single crystal silicon was the subject of several investigations over the past years [12–14]. In summary, radiation damage is known to generate a large excess of vacancies (and other defects) in the crystal. Upon annealing at temperatures above 300 °C, vacancies begin clustering, leading to the formation of He-filled platelets, then evolving to form voids. In parallel, helium outdiffuses with three desorption peaks at 450–500, 650, and 800 °C [9] as its solution enthalpy in silicon is positive (0.84 eV). Annealing at temperatures higher than 600 °C promotes the enlargement of voids and their reshaping to reach their minimum free energy shape (approximately that of a tetrakaidecahedron) We will refer to this type of objects as to *mesovoids*.

The evolution of He–generated vacancies in polysilicon is much less known and elucidated, being obviously dependent upon the pristine micromorphology of the material [15,16]. In the present case, TEM images of polysilicon films before He implantation [Fig. 3(a)] report an in-depth distribution of grain size roughly bimodal, with a top layer, approximately 200–nm thick, characterized by larger lateral grain sizes of about 80 nm; and an inner layer with smaller grains (lateral grain size of ≈ 50 nm) extending for another 250 nm. DF-STEM images relative to films annealed at 1000 °C for two hours in argon show no significant modification of grain size or shape [Fig. 3(b)]. Although possibly surprising, this observation is in good agreement with previous accounts on heavily boron doped polycrystalline silicon, reporting truly marginal grain size variations (if any) at temperatures as high as 900 °C [17]. Also, as reported in previous publications [18], TEM bright field images [Fig. 3(c)] show diffraction contrast details, particularly at GBs, strongly suggesting the formation of boron-rich precipitates (SiB_x).

Samples implanted with He were comparatively analyzed by TEM at the end of each step of Exp2 [Fig. 3(d)–(e)]. While film morphology remains that observed in nHeI, still showing nanograins of ≈ 50 nm in diameter decorated by SiB_x 5-nm precipitates, we found a homogeneous distribution of *nanovoids* with diameters of about 5 nm at 500 °C, either disappearing or shrinking to subnanometric sizes at 1000 °C. Also, mesovoids of irregular shape are observed at GBs. Further analyses about void dynamics in nanocrystalline silicon are reported in a companion paper presented at this Conference [19].

4 Discussion

The set of preliminary evidence just reported confirms that film properties are controlled by the simultaneous occurrence of vacancy and helium diffusion, and of boron diffusion–limited precipitation, leading to the generation of nanovoids and to the formation of a SiB_x second phase.

In the longest processing sequence (Exp1), the variation of the Seebeck coefficient basically reproduces that observed in nHeI specimens submitted to the same annealing sequence. The concurrent increase of σ and α with the annealing temperature properly fits in the framework of carrier energy filtering in two-phase systems [20, 21]. The conductivity is however smaller than in nHeI samples as a combined effect of the damage recovery (at low T_a) and of the residual presence of shrunk nanovoids (at high T_a).

By lowering the duration of the annealing sequence (Exp3) one observes how initially different values of carrier densities in implanted and non-implanted films tend to very similar values for $T_a \geq 800$ °C. The concentration of dissolved (electrically active) boron deeply differs upon He implantation as most of the boron is deactivated by implantation damage . Annealing enables recovery. Also, since it is known that the decrease of carrier density in nHeI samples at high annealing temperatures is due to the partial precipitation of boron to form SiB_x precipitates, the likely evolution of $p(T_a)$ in nHeI and Exp3 samples suggests that precipitation also occurs in Exp3 specimens. This also explains the increase of hole mobility at $T_a \geq 800$ °C, that is accounted for once again by the occurrence of energy filtering in the presence of precipitates. As in Exp1, however, one expects μ values lower than those found in nHeI samples due to the incomplete damage recovery in the low T_a range and to the residual presence of nanovoids at higher T_a.

Finally, the shortest annealing cycle (Exp2) apparently leads to an increase of α over that observed in nHeI films, calling for an effect of sub-nanometric voids. Hall measurements are currently under way. In the absence of carrier density data it may be anyway conjectured that in the depletion region surrounding NVs a lower carrier density (and, as a result, a larger fraction of neutral dopants) would be found. Alternative mechanisms reducing hole density might be related to the large concentration of vacancies made available by the (partially) dissolved voids, thus favoring the formation of boron-vacancy (B_SV_2) complexes that would shift the acceptor level deeper into the energy gap [22]. In both cases the lower carrier density would lead to a larger Seebeck coefficient. Also, since ionized impurity–limited mobility linearly depends on the reciprocal carrier density [23], the reduction of p would be compensated by an increase of μ, thus justifying a conductivity comparable to that observed in nHeI films.

Although no detailed analysis of stability was carried out, based upon data on single-crystalline silicon one may argue that also polycrystalline He–implanted films should be stable up to 800 °C. Actually, between 500 and 800 °C all active processes involving voids are driven by the differential pressure of He in differently sized He-filled voids. Since in samples annealed up to 1000 C helium has already left the voids, no driving force is expected that might cause a micromorphological modification of the material. Thus, one may anticipate that this class of systems might turn out to be of interest also for relatively high temperature applications [24].

5 Conclusions

In this paper we have reported preliminary results concerning the thermoelectric characterization of heavily doped nanocrystalline silicon implanted with He^+. It has been shown that He^+ implantation followed by annealing leads to the formation of nanovoids. Their dynamics was found to drastically differ from that observed in monocrystalline silicon, with much tinier voids forming at 500 °C that further shrink at higher annealing temperatures. Also, thermal processing was found to either not affect or further enhance silicon power factor, leading to a record value of 22 mW $K^{-2}m^{-1}$. Data could be qualitatively explained within the framework of a previously proposed energy–filtering model. Thermal conductivity is currently under measurement and full data on this very promising Si–based system will be reported in forthcoming papers.

References

1. J.A. Carruthers, T.H. Geballe, H.M. Rosenberg, J.M. Ziman, Proc. Royal Soc. **238**, 502 (1957)
2. Y.C. Tai, C.H. Mastrangelo, R.S. Muller, J. Appl. Phys. **63**(5), 1442 (1988)
3. A. Stranz, J. Khler, A. Waag, E. Peiner, J. Electron. Mater. **42**(7), 2381 (2013)
4. D. Narducci, E. Selezneva, A. Arcari, G. Cerofolini, E. Romano, R. Tonini, G. Ottaviani, in *MRS Online Proc. Library, vol. 1314* (MRS, 2011). Mrsf10-1314-ll05-16
5. D. Narducci, E. Selezneva, G. Cerofolini, S. Frabboni, G. Ottaviani, AIP Conf. Proc. **1449**(1), 311 (2012)
6. D. Narducci, E. Selezneva, G. Cerofolini, S. Frabboni, G. Ottaviani, J. Solid State Chem. **193**, 19 (2012)
7. J. Tang, H.T. Wang, D.H. Lee, M. Fardy, Z. Huo, T.P. Russell, P. Yang, Nano Lett. **10**(10), 4279 (2010)

8. J. Boor, D. Kim, X. Ao, M. Becker, N. Hinsche, I. Mertig, P. Zahn, V. Schmidt, Appl. Phys. A **107**(4), 789 (2012)
9. G.F. Cerofolini, G. Calzolari, F. Corni, S. Frabboni, C. Nobili, G. Ottaviani, R. Tonini, Phys. Rev. B **61**, 10183 (2000)
10. L.J. Van Der Pauw, Philips Res. Rep. **13**(1), 1 (1958)
11. C. Wood, A. Chmielewski, D. Zoltan, Rev. Sci. Instrum. **59**(6), 951 (1988)
12. S. Frabboni, F. Corni, C. Nobili, R. Tonini, G. Ottaviani, Phys. Rev. B **69**, 165209 (2004)
13. E. Romano, G.F. Cerofolini, D. Narducci, F. Corni, S. Frabboni, G. Ottaviani, R. Tonini, Surf. Sci. **603**(14), 2188 (2009)
14. V. Raineri, M. Saggio, E. Rimini, J. Mater. Res. **15**(7), 1449 (2000)
15. W. Beyer, R. Carius, U. Zastrow, J. Non-Cryst. Solids **352**(9–20), 1402 (2006)
16. K.J. Abrams, S.E. Donnelly, M.F. Beaufort, J. Terry, L.I. Haworth, D. Alquier, Phys. Status Solidi C **6**(8), 1964 (2009)
17. H.J. Kim, C.V. Thompson, in *MRS Proceedings*, vol. 106 (1987), vol. 106, p. 143
18. D. Narducci, E. Selezneva, G. Cerofolini, E. Romano, R. Tonini, G. Ottaviani, in *Proc. 8th European Thermoelectric Conf.* (CNR, Como, 2010), pp. 141–146
19. B. Lorenzi, S. Frabboni, G. Gazzadi, R. Tonini, G. Ottaviani, D. Narducci, Nanovoid formation and dynamics in He-implanted nanocrystalline silicon, J. Electron. Mater. In press 2014
20. N. Neophytou, X. Zianni, M. Ferri, A. Roncaglia, G. Cerofolini, D. Narducci, J. Electron. Mater. pp. 2393–2401 (2013)
21. N. Neophytou, X. Zianni, H. Kosina, S. Frabboni, B. Lorenzi, D. Narducci, Nanotechnology **24**(20), 205402 (2013)
22. J. Adey, R. Jones, D.W. Palmer, P.R. Briddon, S. Öberg, Phys. Rev. B **71**, 165211 (2005)
23. D. Chattopadhyay, H.J. Queisser, Rev. Mod. Phys. **53**(4), 745 (1981)
24. S. Kumar, S. Heister, X. Xu, J. Salvador, G. Meisner, J. Electron. Mater. **42**(4), 665 (2013)

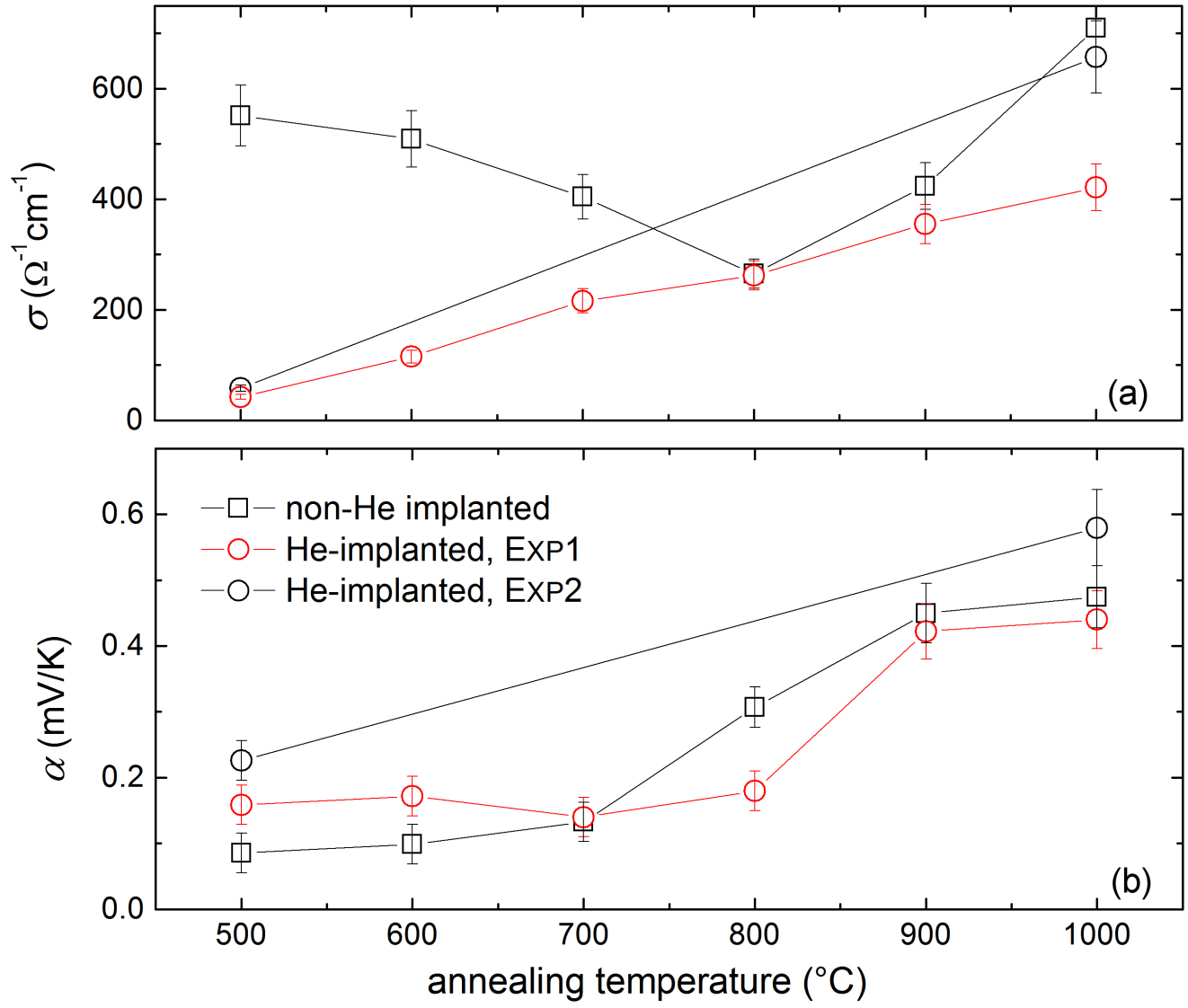
σ (Ω⁻¹cm⁻¹)
600
400
200
0
(a)
non-He implanted
He-implanted, EXP1
He-implanted, EXP2
α (mV/K)
0.6
0.4
0.2
0.0
(b)
500
600
700
800
900
1000
annealing temperature (°C)

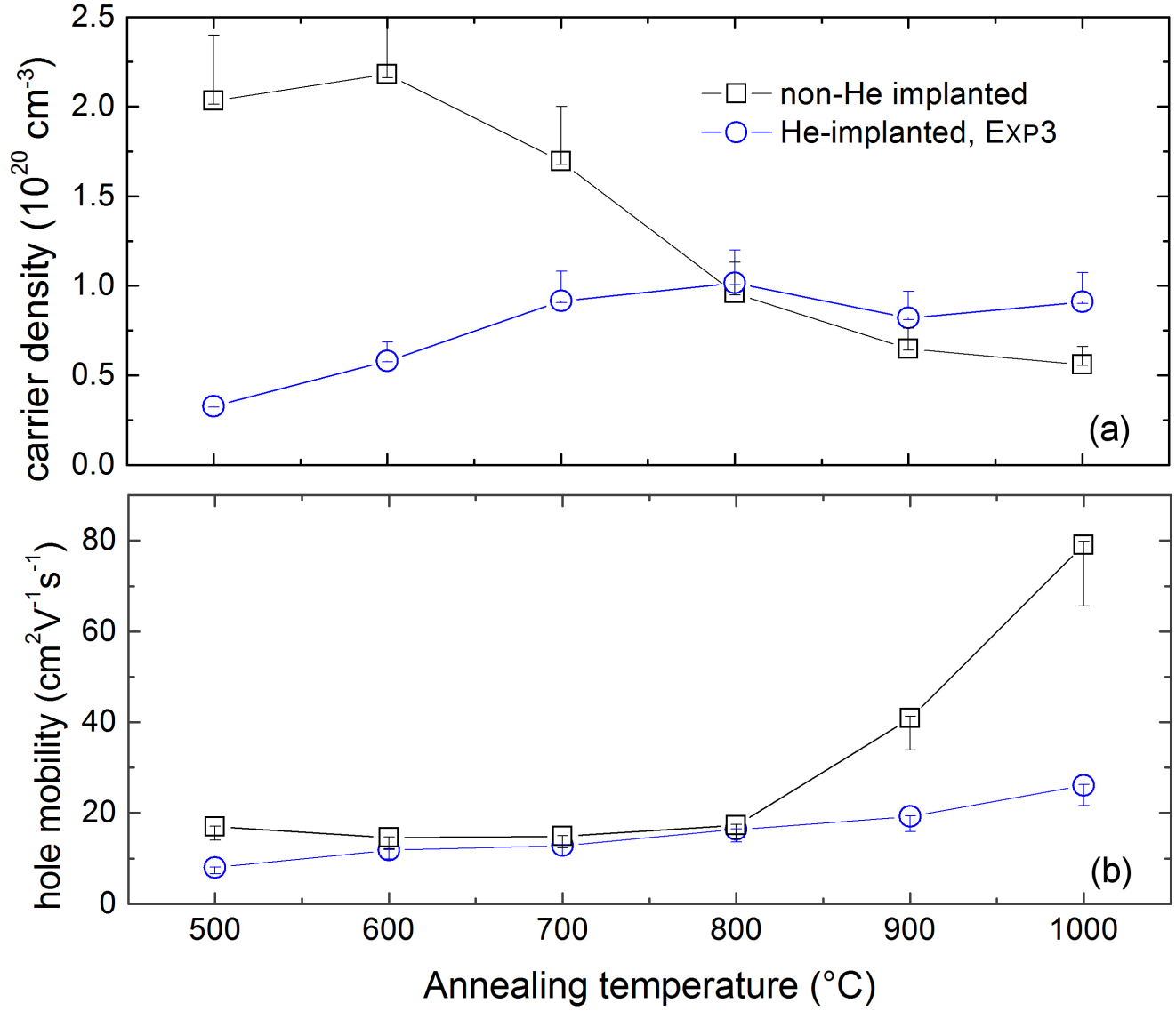
carrier density (10^{20} cm^{-3})
2.5
2.0
1.5
1.0
0.5
0.0
non-He implanted
He-implanted, EXP3
(a)
hole mobility (cm^{2}V^{-1}s^{-1})
80
60
40
20
0
(b)
500
600
700
800
900
1000
Annealing temperature (°C)

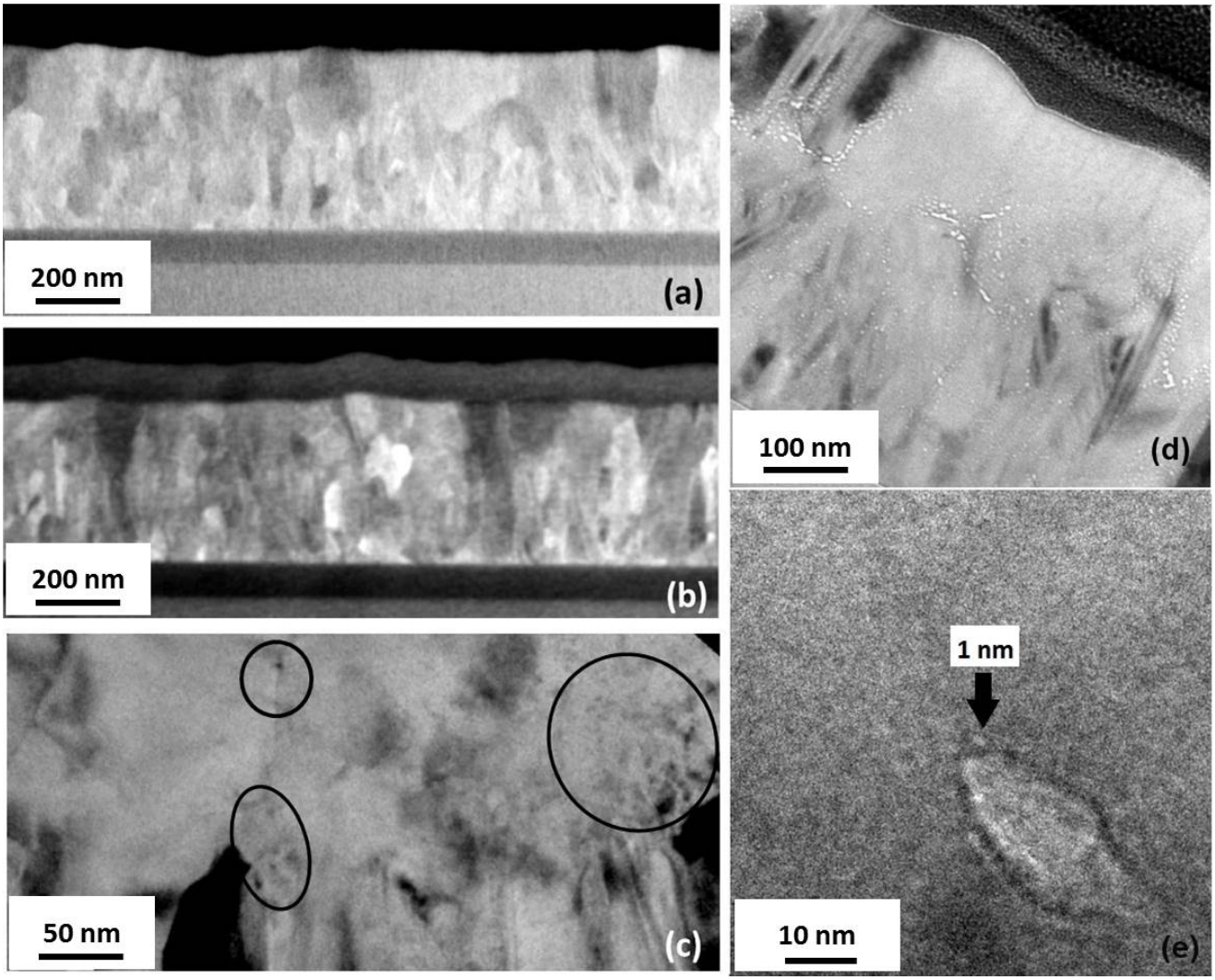
200 nm
(a)
200 nm
(b)
50 nm
(c)
100 nm
(d)
1 nm
10 nm
(e)